solubility of AlCp* in benzene and its extreme sensitivity to moisture and air.

The theoretical ^{27}Al NMR chemical shifts for the monomer and tetramer of AlCp* allow an assignment of the NMR signal at -80 ppm to the tetramer (cf. Figure 5). The estimated value of -85 ppm for the tetramer, which is obtained by adding the difference between the chemical shifts of AlCp* and AlCp to the δ value of Al_4Cp_4 (cf. Table II), agrees very well with the experimental value, while for the monomer an even more shielded value of -143 ppm is obtained in the calculations. Therefore, the tetrameric units of the solid phase are preserved in solution and, at least at low temperature, no experimental evidence for the monomer of AlCp* exists.

Since the calculated tetramerization energy of AlCp (about 150-160 kJ/mol[14]) is rather low and since a similar value can be expected for AlCp*, we have tried to observe the dissociation of $Al_4Cp^*_4$ by increasing the temperature and monitoring the ^{27}Al NMR spectrum. Indeed, above 30 °C a new signal at -149.5 ppm is observed, which, according to the quantum chemical calculations (cf. Figure 5 and Table II; the calculated value is -143 ppm), can be attributed to the AlCp* monomer.

By further increasing the temperature, the new peak at -149.5 ppm is growing in intensity, while at the same time the intensity of the original peak is more and more decreased. An analysis of the intensity ratios at 60, 80, and 100 °C yields for the tetramerization energy ($\Delta H°$) an estimate of about 150 ± 20 kJ/mol, which is of same magnitude as the value predicted for AlCp by ab initio calculations.[14]

In the case of AlCp*, the combination of ^{27}Al NMR spectroscopy with quantum chemical ab initio calculations of chemical shifts leads to a detailed characterization of the solution of $Al_4Cp^*_4$ crystals in toluene and provides for the first time evidence for the existence of monomeric AlCp*. Finally, it should be noted that solvation effects turn out to be negligible for AlCp*. Test calculations of $AlCp{\cdot}H_2O$ complexes showed that the latter are only weakly bonded and that the chemical shifts are at most affected by 5-10 ppm, as expected by the σ-π model, much less than the estimated accuracy of our calculations.

Using the same procedure as we have just described for AlCp*, it should be possible to investigate the structure of a solution of AlCp in toluene/ether. The latter can be prepared in the same way as AlCp*,[5] by reaction of AlCl in a mixture of toluene and ether as solvent with $MgCp_2$. However, AlCp is only stable up to -60 °C and disproportionates at higher temperatures. Therefore, it was not possible to carry out a temperature-dependent NMR study, and we could only obtain the ^{27}Al NMR spectrum at -80 °C. The latter shows one signal at -111 ppm, which, according to the quantum chemical calculations (cf. Table II), can be assigned to the tetramer. The calculated value for Al_4Cp_4 is -105 ppm, while the corresponding value for the monomer is predicted to be -172 ppm. Due to the thermal instability of AlCp, no experimental evidence for the existence of the monomer of AlCp could be obtained so far.

V. Conclusions

We have shown that experimental NMR spectra of Al^I compounds in solution can be interpreted on the basis of theoretical calculation of ^{27}Al chemical shifts. This approach has been proven particularly successful in the case of AlCp*, where theoretical calculations allowed an unambiguous identification of tetrameric and monomeric species in solution. Theoretical calculations were furthermore the basis of a thorough investigation of the dissociation of $Al_4Cp^*_4$ into 4AlCp*. In addition, first evidence for the existence of the AlCp* monomer in solution has been obtained on the basis of the theoretical predictions.

The given examples add further support to the power of theoretical NMR shift calculations concerning the interpretation of experimental spectra of hithero unknown compounds. In particular, chemical shift calculations are an invaluable tool for the interpretation of experimental spectra if there are no other experimental NMR data available for comparison, as in the case of the Al^I compounds.

Acknowledgment. This work was supported by the Fonds der Chemischen Industrie, in particular through a "Liebig-Stipendium" to J.G. which is gratefully acknowledged.

Molecular Modeling of the Kinetic Isotope Effect for the [1,5] Sigmatropic Rearrangement of *cis*-1,3-Pentadiene

Yi-Ping Liu,[†] Gillian C. Lynch,[†] Thanh N. Truong,[†] Da-hong Lu,[†] Donald G. Truhlar,*[,†] and Bruce C. Garrett[‡]

Contribution from the Department of Chemistry and Supercomputer Institute, University of Minnesota, Minneapolis, Minnesota 55455-0431, and Molecular Sciences Research Center, Pacific Northwest Laboratory, Richland, Washington 99352. *Received June 8, 1992*

Abstract: The primary kinetic isotope effect for the [1,5] sigmatropic rearrangement reaction of *cis*-1,3-pentadiene is studied by the direct dynamics method. The calculations are carried out with the computer code MORATE, which combines the semiempirical molecular orbital package, MOPAC, and the polyatomic dynamics code, POLYRATE, developed previously by our research group. Dynamics calculations are based on canonical variational transition-state theory including multidimensional tunneling corrections. The force field is obtained by molecular orbital theory with the AM1, PM3, and MINDO/3 parameterizations. The kinetic isotope effects calculated with the MINDO/3 and PM3 Hamiltonians agree with those calculated by AM1 within 13%, and the latter agree with experiment within 13%. The tunneling contributions to the kinetic isotope effects are analyzed, and the nature of the vibrationally assisted tunneling process is discussed. General features of the dynamics from all three parameterizations are similar, and the quantitative differences in the predictions of the three calculations can be understood in terms of global characteristics of the potential energy functions that they predict.

Introduction

Reactions involving transfer or migration of hydrogen atoms, protons, and hydride ions often involve tunneling,[1] and realistic calculations of tunneling processes require at least a semiglobal potential energy function (PEF).[2] Analytic representation of PEFs (i.e., potential surface fitting)[3] is a difficult, time-consuming,

[†] University of Minnesota.
[‡] Molecular Sciences Research Center.

(1) (a) Skodje, R. T.; Truhlar, D. G.; Garrett, B. C. *J. Chem. Phys.* **1982**, *77*, 5955. (b) Kreevoy, M. M.; Truhlar, D. G. In *Investigation of Rates and Mechanisms of Reaction* ("Techniques of Chemistry", 4th ed.); Bernasconi, C. F., Ed.; John Wiley & Sons: New York, 1986; Part 1, p 13.

0002-7863/93/1515-2408$04.00/0

and expensive proposition for most organic systems, and in many cases this (more than the difficulty of the dynamical calculations themselves) has prevented interesting applications of modern dynamical theory to organic and biochemical reactions. In this paper we present a semiclassical tunneling calculation on the hydrogen shift reaction of *cis*-1,3-pentadiene which uses semiempirical molecular orbital theory[4,5] as an alternative to the analytic representation of the PEF. This kind of calculation, in which electronic structure calculations of energies and gradients are performed as needed rather than as input to a fitting step that precedes the dynamics calculations (so that the PEF is only implicit), is called direct dynamics.[6] Such calculations are facilitated (i) by the availability of parameterized models (e.g., MINDO/3,[5a] AM1,[5b] and PM3[5c]) which provide good general-purpose parameters to serve as implicit PEFs for selected reactions, and (ii) by variational transition-state theory[7-9] including multidimensional semiclassical tunneling contributions,[2d,7,9] because this kind of theory reduces the dynamics to contributions from reasonably localized regions of configuration space. The present dynamics calculations are based on canonical variational theory[7,8] (CVT) and the centrifugal-dominant small-curvature tunneling (SCT) approximation,[9] which should be valid because reaction-path curvature is found to be small over the region important for tunneling. All calculations were carried out with a new computer program, MORATE,[10] and we carried out calculations with the electronic Hamiltonian approximated by each of the three parameterized methods mentioned above.

The [1,5] sigmatropic rearrangement reaction of *cis*-1,3-pentadiene has been studied extensively.[11-18] Experimental measurements show that the primary kinetic isotope effect (KIE) is large (≈5) and exhibits a strong temperature dependence even at fairly high temperatures (~460–500 K).[11] Conventional transition-state theory with a classical treatment of reaction-coordinate motion does not reproduce this trend.[13-15] There has been some controversy about the role of tunneling in [1,5] sigmatropic rearrangements, with arguments pro and con.[13-22] Tunneling can only be attributed to vibrational motions for this reaction since there is no relative translational motion in a unimolecular reaction. The rearrangement involves an internal rotational motion to transform the starting *s-trans* conformation to the transition state, and Dewar et al.[15] proposed a model in which this motion is classical, but the hydrogen migration occurs by tunneling. Their calculated KIE of 146 at 498 K is in poor agreement with experiment. Chantranupong and Wildman[18] used a two-mode tunneling model in which the transfer is approximated as collinear. The reduced mass of the second mode was fixed at a value typical of the various low-frequency modes of the reactant, and its frequency was varied to reproduce the observed KIE.

In the present treatment, all 33 internal degrees of freedom are included in the tunneling calculation with their correct reduced mass, the reaction is correctly described as noncollinear, in particular suprafacial,[23] and all geometries, energies, gradients, and frequencies are computed as functions of the reaction coordinate directly from the implicit PEF. The tunneling probabilities are calculated by an improved small-curvature tunneling approximation, called the centrifugal-dominant small-curvature semiclassical adiabatic ground-state method (CD-SCSAG) or, for short, the small-curvature tunneling (SCT) method. We present results for the specific isotopomers studied experimentally, in particular for the ratio of the reaction rate (k_H) for D_2C–$(CH)_3$–CH_3 to that (k_D) for H_2C–$(CH)_3$–CD_3.

The reaction under consideration involves the migration of a light atom, H or D, between two carbon centers. For bimolecular reactions this heavy–light–heavy mass combination always involves large curvature of the reaction path,[7] but for unimolecular reactions the reaction-path curvature may be either large or small. We have calculated the reaction path, and we have calculated tunneling amplitudes both for the tunneling path that dominates in the small-curvature limit and for the kind that dominates in the large-curvature limit. We found that the system is closer to the small-curvature limit. Thus we use the SCT tunneling method for the final calculations presented here. The new CD-SCSAG approximation[9] for small-curvature tunneling is an improvement over the original[24] SCSAG small-curvature method in that it accounts for the effect of mode–mode coupling on the extent of corner cutting[7,25,26] through each vibrational degree of freedom orthogonal to the reaction path.

This paper is organized as follows. A brief review of variational transition-state theory (VTST) and a presentation of the small-curvature tunneling approximation are given in the Theory section. Details of the calculations are given in the Computational Section. Subsequent sections give results, discussion, and conclusions. Comparisons with earlier calculations[15,18] are presented in the Discussion section.

Theory

Variational Transition-State Theory. The variational transition-state theory rate constant is the minimized value obtained

(2) (a) Johnston, H. G. *Gas Phase Reaction Rate Theory*; Ronald Press: New York, 1966. (b) Truhlar, D. G.; Kuppermann, A. *J. Chem. Phys.* **1972**, *56*, 2232. (c) Truhlar, D. G.; Brown, F. B.; Steckler, R.; Isaacson, A. D. In *The Theory of Chemical Reaction Dynamics*; Clary, D. C., Ed.; Reidel: Dordrecht, 1986; p 285. (d) Truhlar, D. G.; Garrett, B. C. *J. Chim. Phys.* **1987**, *84*, 365.

(3) Truhlar, D. G.; Steckler, R.; Gordon, M. S. *Chem. Rev.* **1987**, *87*, 217.

(4) Pople, J. A.; Beveridge, D. L. *Approximate Molecular Orbital Theory*; McGraw-Hill: New York, 1970. Flanigan, M. C.; Kumornicki, A.; McIver, J. W., Jr. In *Semiempirical Methods of Electronic Structure Calculation, Part B*; Segal, G. A., Ed.; Plenum: New York, 1977; p 1. Dewar, M. J. S.; Thiel, W. *J. Am. Chem. Soc.* **1977**, *99*, 4899.

(5) (a) Bingham, R. C.; Dewar, M. J. S.; Lo, D. H. *J. Am. Chem. Soc.* **1975**, *97*, 1285. (b) Dewar, M. J. S.; Zoebisch, E. G.; Healy, E. F.; Stewart, J. J. P. *J. Am. Chem. Soc.* **1985**, *107*, 3902. (c) Stewart, J. J. P. *J. Comput. Chem.* **1989**, *10*, 209, 221.

(6) Doubleday, C. J.; McIver, J. W., Jr.; Page, M. *J. Phys. Chem.* **1988**, *92*, 4367. Baldridge, K. K.; Gordon, M. S.; Steckler, R.; Truhlar, D. G. *J. Phys. Chem.* **1989**, *93*, 5107. Truhlar, D. G.; Gordon, M. S. *Science* **1990**, *249*, 491. Gonzalez-Lafont, A.; Truong, T. N.; Truhlar, D. G. *J. Phys. Chem.* **1991**, *95*, 4618.

(7) (a) Truhlar, D. G.; Isaacson, A. D.; Garrett, B. C. In *Theory of Chemical Reaction Dynamics*; Baer, M., Ed.; CRC Press: Boca Raton, FL, 1985; Vol. 4, p 65. (b) Garrett, B. C.; Truhlar, D. G. *Annu. Rev. Phys. Chem.* **1984**, *35*, 159. (c) Tucker, S. C.; Truhlar, D. G. In *New Theoretical Concepts for Understanding Organic Reactions*; Bertran, J., Csizmadia, I. G., Eds.; Kluwer Academic Publishers: Dordrecht, 1989; p 291.

(8) Garrett, B. C.; Truhlar, D. G. *J. Chem. Phys.* **1979**, *70*, 1593.

(9) Lu, D.-h.; Truong, T. N.; Melissas, V. S.; Lynch, G. C.; Liu, Y.-P.; Garrett, B. C.; Steckler, R.; Isaacson, A. D.; Rai, S. N.; Hancock, G. C.; Lauderdale, J. G.; Joseph, T.; Truhlar, D. G. *Comput. Phys. Commun.* **1992**, *71*, 235.

(10) Truong, T. N.; Lu, D.-h.; Lynch, G. C.; Liu, Y.-P.; Melissas, V. S.; Stewart, J. J. P.; Steckler, R.; Garrett, B. C.; Gonzalez-Lafont, A.; Rai, S. N.; Hancock, G. C.; Joseph, T.; Truhlar, D. G. *Comput. Phys. Commun.*, in press.

(11) Roth, W. R.; König, J. *Liebigs Ann. Chem.* **1966**, *699*, 24.

(12) Bingham, R. C.; Dewar, M. J. S. *J. Am. Chem. Soc.* **1972**, *94*, 9107.

(13) Hess, B. A., Jr.; Schaad, L. J. *J. Am. Chem. Soc.* **1983**, *105*, 7185. Hess, B. A., Jr.; Schaad, L. J.; Pancíř, J. *J. Am. Chem. Soc.* **1985**, *107*, 149.

(14) Rondan, N. G.; Houk, K. N. *Tetrahedron Lett.* **1984**, *25*, 2519. Kahn, S. D.; Hehre, W. J.; Rondan, N. G.; Houk, K. N. *J. Am. Chem. Soc.* **1985**, *107*, 8291. Jensen, F.; Houk, K. N. *J. Am. Chem. Soc.* **1987**, *109*, 3139.

(15) Dewar, M. J. S.; Merz, K. M., Jr.; Stewart, J. J. P. *J. Chem. Soc., Chem. Commun.* **1985**, 166.

(16) Dewar, M. J. S.; Healy, E. F.; Ruiz, J. M. *J. Am. Chem. Soc.* **1988**, *110*, 2666.

(17) Dormans, G. J. M.; Buck, H. M. *J. Mol. Struct.* **1986**, *136*, 121; *J. Am. Chem. Soc.* **1986**, *108*, 3253.

(18) Chantranupong, L.; Wildman, T. A. *J. Am. Chem. Soc.* **1990**, *112*, 4151.

(19) Spangler, C. W. *Chem. Rev.* **1976**, *76*, 187.

(20) Kwart, H.; Brechbiel, M. W.; Acheson, R. M.; Ward, D. C. *J. Am. Chem. Soc.* **1982**, *104*, 4671. Kwart, H. *Acc. Chem. Res.* **1982**, *15*, 401.

(21) Shen, G.-Y.; Tapia, R.; Okamura, W. H. *J. Am. Chem. Soc.* **1987**, *109*, 7499.

(22) Pegg, G. C.; Meehan, G. V. *Aust. J. Chem.* **1990**, *43*, 1071.

(23) Woodward, R. B.; Hoffmann, R. *The Construction of Orbital Symmetry*; Verlag Chemie: Weinhein, FRG, 1970.

(24) Skodje, R. T.; Truhlar, D. G.; Garrett, B. C. *J. Phys. Chem.* **1981**, *85*, 3019.

(25) Marcus, R. A. *J. Chem. Phys.* **1966**, *45*, 4493.

(26) (a) Kuppermann, A.; Adams, J. T.; Truhlar, D. G. *Abstr. Pap. Int. Conf. Phys. Electron. At. Collisions, 8th* **1973**, 149. (b) Marcus, R. A.; Coltrin, M. E. *J. Chem. Phys.* **1977**, *67*, 2609. (c) Skodje, R. T.; Truhlar, D. G.; Garrett, B. C. *J. Chem. Phys.* **1982**, *77*, 5955.

by varying the location of the transition state along a reference path.[8] This minimizes the error due to "recrossing" trajectories.[7,27] The choice we make for the reference path is the minimum energy path (MEP) obtained by following the path of steepest descent of the potential from the saddle point in a mass-scaled Cartesian coordinate system,[25,28-31] scaled to a reduced mass μ. (In the present paper we set μ equal to 1 amu. This arbitrary choice has absolutely no effect on calculated observables, but choosing a physical value makes distances in the mass-scaled system correspond more closely to physical distances.) We define the distance along the MEP through mass-scaled coordinates as s, which is zero at the saddle point and is negative and positive on the reactant and product sides, respectively, and we define the Born–Oppenheimer potential on the MEP at s as $V_{MEP}(s)$. For a canonical ensemble at a given temperature T, the hybrid (i.e., classical reaction path motion with other degrees of freedom quantized) canonical variational theory (CVT) rate constant for a bimolecular reaction is given by[7]

$$k^{CVT}(T) = \min_s k^{GT}(T,s) = \sigma\frac{\tilde{k}T}{h}\frac{Q^{GT}(T,s_*^{CVT})}{Q^R(T)}\exp(-V_{MEP}^{CVT}/\tilde{k}T) \quad (1)$$

where the superscript GT denotes a generalized transition-state theory expression, s_*^{CVT} is the temperature-dependent value of s at which k^{GT} has a minimum; i.e., the location of the CVT transition state, σ is the symmetry factor (omitted from rotational partition functions) which accounts for the reaction path multiplicity, $\tilde{k}$ is the Boltzmann constant, h is Planck's constant, V_{MEP}^{CVT} is the Born–Oppenheimer potential on the MEP at s_*^{CVT}, $Q^{GT}(T,s_*^{CVT})$ is the internal quantized partition function for a generalized transition state (GTS) at $s = s_*^{CVT}$ with V_{MEP}^{CVT} as the local zero of the energy, and Q^R is the reactant quantum partition function with respect to the overall zero of energy taken as the equilibrium potential of the reactant for a unimolecular reaction or of reactants infinitely apart for bimolecular reactions. If the generalized transition state is located at the saddle point ($s = 0$) instead of the variationally optimized s_*^{CVT}, then V_{MEP}^{CVT} is replaced by the classical barrier height V^*, and eq 1 reduces to conventional transition-state theory.

To include quantum effects for motion along the reaction coordinate, we multiply $k^{CVT}(T)$ by a ground-state transmission coefficient,[27,32] $\kappa^{CVT/G}$, which primarily corrects for the influence of tunneling on the rate constant and for nonclassical reflection effects. The final quantized rate constant is

$$k^{CVT/G}(T) = \kappa^{CVT/G}(T)k^{CVT}(T) \quad (2)$$

For small reaction-path curvature, the effective potential for tunneling is the vibrationally adiabatic ground-state potential curve[30,32,33] defined by

$$V_a^G(s) = V_{MEP}(s) + \epsilon_{int}^G(s) \quad (3)$$

where $\epsilon_{int}^G(s)$ denotes the zero-point energy in vibrational modes transverse to the MEP. The ground-state transmission coefficient, $\kappa^{CVT/G}(T)$, is defined as the ratio of the thermally averaged quantal transmission probability, $P^G(E)$, for reaction in the ground state, to the thermally averaged classical transmission probability, $P_C^{CVT/G}(E)$ implicit in k^{CVT} for classical reaction-coordinate motion along the one-dimensional ground-state effective potential, i.e.,

$$\kappa^{CVT/G}(T) = \frac{\int_0^\infty P^G(E)e^{-E/\tilde{k}T}dE}{\int_0^\infty P_C^{CVT/G}(E)e^{-E/\tilde{k}T}dE} \quad (4)$$

where $P_C^{CVT/G}(E)$ is zero when the energy of the system is below the classical threshold energy, $V_a^G(s=s_*^{CVT})$, implied by hybrid canonical variational theory. Carrying out the integral in the denominator, eq 4 becomes,

$$\kappa^{CVT/G}(T) = \frac{1}{\tilde{k}T}\exp\left[\frac{1}{\tilde{k}T}V_a^G(s=s_*^{CVT})\right]\int_0^\infty P^G e^{-E/\tilde{k}T}dE \quad (5)$$

We define $V_{MEP}(s=s^R)$ to be zero, where s^R is a negative value of s corresponding to reactants. It is useful for interpretative purposes to also define a version of the vibrationally adiabatic ground-state potential curve that goes to zero at the reactant geometry. This is given by

$$\Delta V_a^G(s) = V_a^G(s) - \epsilon_{int}^G(s=s^R) \quad (6)$$

Centrifugal-Dominant Small-Curvature Ground-State Tunneling Method.[9] Several semiclassical tunneling approximations are available to calculate $P^G(E)$.[1,7,9,24,32] The minimum energy path semiclassical adiabatic ground-state (MEPSAG) method[30,32] assumes that the reaction path has negligible curvature so that the tunneling path essentially coincides with it. Transmission coefficients $\kappa^{CVT/G}(T)$ calculated by this method are labeled ZCT ("zero-curvature tunneling").

However, tunneling occurs on the concave side of the MEP when the reaction path possesses curvature.[1a,2c,d,7,25,26] The centrifugal-dominant small-curvature semiclassical adiabatic ground-state (CD-SCSAG) approximation is a generalization of the Marcus–Coltrin approximation[26b] in which the tunneling path is distorted from the MEP out to a concave-side vibrational turning point in the direction of the internal centrifugal force.[9] Instead of defining the tunneling path, the centrifugal effect is included by replacing the reduced mass by an effective reduced mass, $\mu_{eff}(s)$, which is used to evaluate imaginary action integrals and thereby tunneling probabilities. The ground-state transmission probability at energy E is

$$P^G(E) = 1/\{1 + \exp[-2\theta(E)]\} \quad (7)$$

where $\theta(E)$ is the imaginary action integral evaluated along the tunneling path,

$$\theta(E) = (2\pi/h)\int_{s_0}^{s_1}\sqrt{2\mu_{eff}(s)|E - V_a^G(s)|}\,ds \quad (8)$$

and where the integration limits are reaction-coordinate turning points defined by

$$V_a^G[s_0(E)] = V_a^G[s_1(E)] = E \quad (9)$$

The effect of the reaction-path curvature is included in the effective reduced mass as explained below. The small-curvature tunneling amplitude corresponds approximately to an implicit tunneling path that follows the line of concave-side vibrational turning points at a distance $\bar{l}(s)$ from the MEP in the direction of the reaction-path curvature vector. Let the distance along the small-curvature tunneling path be ξ and the curvature at s be $\kappa(s)$; then it is easily shown by analytic geometry that

$$d\xi = \left\{[1 - \kappa(s)\bar{l}(s)]^2 + \left(\frac{d\bar{l}(s)}{ds}\right)^2\right\}^{1/2}ds \quad (10)$$

The imaginary action integral is defined as

$$\theta(E) = (2\pi/h)\int\sqrt{2\mu|E - V_a^G[s(\xi)]|}\,d\xi \quad (11)$$

By comparing eq 8 and eq 11, the effective reduced mass is given by

$$\mu_{eff}(s) = \mu\{[1 - \kappa(s)\bar{l}(s)]^2 + [d\bar{l}(s)/ds]^2\} \quad (12)$$

However, to make the method generally applicable even when $\bar{l}(s)$

(27) Truhlar, D. G.; Garrett, B. C. *Acc. Chem. Res.* **1980**, *13*, 440.
(28) Shavitt, I. Theoretical Chemistry Laboratory Report No. WIS-AEC-23; University of Wisconsin: Madison, 1959.
(29) Marcus, R. A. *J. Chem. Phys.* **1964**, *41*, 610.
(30) Truhlar, D. G.; Kuppermann, A. *J. Am. Chem. Soc.* **1971**, *93*, 1840.
(31) Fukui, K. In *The World of Quantum Chemistry*; Daudel, R., Pullman, B., Eds.; Reidel: Dordrecht, Holland, 1974; p 113.
(32) Garrett, B. G.; Truhlar, D. G.; Grev, R. S.; Magnuson, A. W. *J. Phys. Chem.* **1980**, *84*, 1730.
(33) Marcus, R. A. *J. Chem. Phys.* **1967**, *46*, 959. Truhlar, D. G. *J. Chem. Phys.* **1970**, *53*, 2041.

Table I. Energetics[a] (kcal/mol)

				$D_2C(CH)_3CH_3$		$H_2C(CH)_3CD_3$	
	s-cis	$\phi_1 = 0$	V^*	$V_a^G(s_*^{CVT})$	$\Delta V_a^G(s_*^{CVT})$	$V_a^G(s_*^{CVT})$	$\Delta V_a^G(s_*^{CVT})$
MINDO/3		1.3[b]	45.7[b]	112.1	43.6	111.0	44.3
AM1	1.1[c]	1.7[b]	39.5[b]	105.5	37.9	104.3	38.5
PM3	1.9[c]	2.3[b]	36.6[b]	100.3	33.8	99.3	34.7

[a] The energetics tabulated are energies with respect to the energy of the *s-trans* conformation. [b] Saddle point, i.e., one imaginary frequency. [c] Local minimum.

is greater than or equal to the radius of curvature of the reaction path, we calculate the effective reduced mass by[24]

$$\mu_{eff}(s) = \mu f(s) \tag{13}$$

where the function $f(s)$ is defined such that eq 13 agrees with eq 12 through leading terms but is not singular, in particular,

$$f(s) = \min\begin{cases}\exp\left[-2\kappa(s)\bar{t}(s) - [\kappa(s)\bar{t}(s)]^2 + (d\bar{t}(s)/ds)^2\right] \\ 1\end{cases} \tag{14}$$

The evaluation of $\bar{t}(s)$ is explained in detail elsewhere[9] and will not be repeated here.

Transmission coefficients $\kappa^{CVT/G}(T)$ calculated by the CD-SCSAG method are labeled SCT ("small-curvature tunneling").

Computational Section

The stationary points are optimized using the MOPAC program.[34] Dynamics calculations are performed using the MORATE program,[10] in particular, version 4.5/P4.5.1-M5.03. In all cases, the SCF convergence criterion (i.e., SCFCRT[34]) is set to 1×10^{-11}.

Gradients needed for the dynamics calculations are obtained from MOPAC, and the Hessians are obtained by taking central differences of the gradients. The step size used for the central difference calculation is determined by matching the vibrational frequencies at the stationary points to the results obtained from FORCE calculations carried out with MOPAC for each isotopic variation of the reaction. For the given central difference step size, the dynamics calculations are converged within 2%.

The Page–McIver method[35,36] is employed to calculate the MEP. Vibrations are treated harmonically. Other computational details are explained elsewhere.[7a,9,10]

We present results on the ratio of the reaction rate (k_H) for $D_2C-(CH)_3-CH_3$ to that (k_D) for $H_2C-(CH)_3-CD_3$. The reason for choosing these isotopomers is that they are the ones studied experimentally;[10] we note that there is a (presumably small) secondary KIE along with the primary KIE.

Results

Conformation Analysis. The reactant is the *s-trans* conformer. For all three electronic Hamiltonians, MINDO/3, AM1, and PM3, that conformer has the lowest energy, and it has a C1–C2–C3–C4 dihedral angle (ϕ_1) of 180°. We varied ϕ_1 from 0 to 180° and optimized all the other internal degrees of freedom for each value of ϕ_1; this yields the internal rotation potential energy profiles shown in Figure 1. The complicated shapes of these profiles reflect a competition between steric factors that would lead to a monotonically decreasing function and π conjugation that would lead to minima at both $\phi_1 = 0$ and 180°. The MINDO/3 Hamiltonian does not show an *s-cis* minimum (we refer to the lowest minimum with $\phi_1 < 90°$ as *s-cis* even if ϕ_1 is not 0; some might prefer the word *gauche* or cisoid in this case), whereas AM1 does (although not at $\phi_1 = 0$), and PM3 shows two (neither at $\phi_1 = 0$). Table I gives the energies of the $\phi_1 = 0$ geometries and the lowest *s-cis* local minima. These minima occur at ϕ_1 equal to 35° and 60° for AM1 and PM3, respectively.

Saddle Point. The calculated classical barrier heights are given in the V^* column of Table I. The structure at the saddle point has C_s symmetry for all three semiempirical models. This agrees with the best previous calculations.[13,14,16] The three parameterized models predict similar structures for the saddle point, with all bond distances agreeing within 0.09 Å and all bond angles agreeing within 13°. The C1–C2–C3–C4 dihedral angle ϕ_1 and the C2–C3–C4–C5 dihedral angle ϕ_2 are equal to one another at the saddle point, where they have the values 9, 16, or 17° for the MINDO/3, AM1, or PM3 level of theory, respectively.

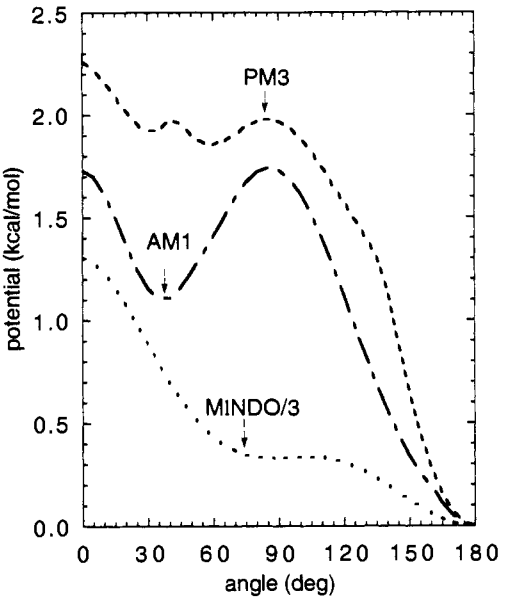

Figure 1. The potential energy profiles corresponding to rotating the C1–C2 vinyl group around the C2–C3 single bond.

Table II. Rate Constants (cm^3 molecule^{-1} s^{-1}) and Transmission Coefficients for $D_2C(CH)_3CH_3$ at 470 K

			$\kappa^{CVT/G}$		
	k^*	k^{CVT}	ZCT	SCT	$k^{CVT/SCT}$
MINDO/3	5.7×10^{-10}	5.7×10^{-10}	2.5	4.5	2.6×10^{-9}
AM1	1.9×10^{-7}	1.8×10^{-7}	4.2	6.5	1.2×10^{-6}
PM3	1.5×10^{-4}	1.5×10^{-4}	4.4	5.4	7.8×10^{-4}

Variational Transition States, Rate Constants, and Transmission Coefficients. Table I also lists the adiabatic ground-state potential $V_a^G(s_*^{CVT})$ at the CVT transition state at 470 K, and it lists $\Delta V_a^G(s_*^{CVT})$, which equals the previous quantity minus the reactant adiabatic ground-state potential energy as indicated in eq 6. The zero-point contribution to the effective barrier, which equals $\Delta V_a^G - V^*$, ranges from −1.0 to −2.8 kcal/mol in the various cases.

Table II gives, for the H-migration case, rate constants calculated with unit transmission coefficients by conventional transition-state theory and canonical variational theory, transmission coefficients calculated without considering reaction path curvature and also by the SCT method, and the final rate constants calculated by eq 2. Figure 2 shows the three calculated rate constants for the D-migration reaction at the highest temperature at which the kinetic isotope effect was directly measured. Clearly the absolute rate constant is very dependent on the barrier height. Visual inspection of Figure 2 indicates that the correct barrier height (i.e., the value that would make the calculated rate constants agree best with experiment) is about 38 kcal/mol.

In all cases, the variational effect on the transition-state location is negligible; i.e., the dynamical bottleneck of each reaction is at or very close to its saddle point. As a consequence, k^{CVT} is very close to k^*; i.e., little recrossing of the saddle point dividing surface is predicted.

(34) Stewart, J. J. P. MOPAC Program, Version 5.0; Frank J. Sieler Research Laboratory, U.S. Air Force Academy, 1989.
(35) Page, M.; McIver, J. W., Jr. *J. Chem. Phys.* **1988**, *88*, 922.
(36) Melissas, V. S.; Truhlar, D. G.; Garrett, B. G. *J. Chem. Phys.* **1992**, *96*, 5758.

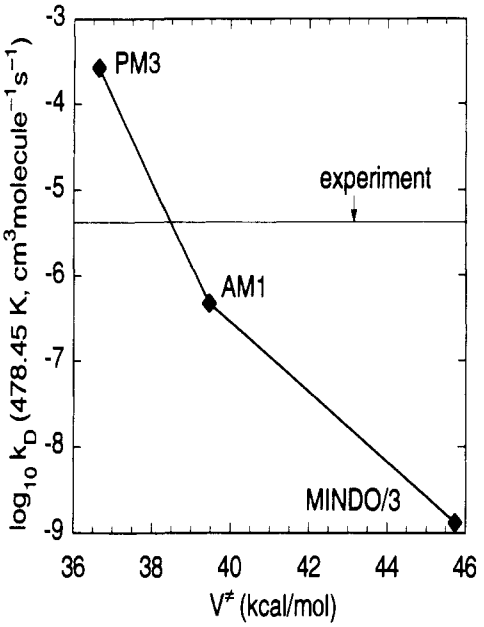

Figure 2. Calculated (CVT/SCT) and experimental rate constants for the D transfer reaction at 478.45 K.

Table III. k_H/k_D

	CVT/SCT			TST[a]	CW[b]	
T (K)	MINDO/3	AM1	PM3	MINDO/2	AM1	expt
463.25	4.5	5.2	5.7		5.1	5.3
470	4.3	4.9	5.5	2.5	4.9	5.2
478.45	4.2	4.7	5.2		4.7	5.0
500	3.8	4.1	4.6	2.4	4.2	4.7

[a] TST is from ref 15. [b] Obtained by spline interpolation of the results in ref 18.

Kinetic Isotope Effects. Table III contains the calculated KIEs for the three molecular orbital models and compares them to previous calculations and to experiment. Considering the differences in barrier height and saddle point geometries, it is interesting to see that all three parameterized models tested here lead to reasonable agreement with the experimental KIEs.

Although the direct effect of the barrier height cancels out in the kinetic isotope effect, one expects in general that the indirect effect of the calculated barrier height can be appreciable. For example, for significantly exothermic reactions, higher barriers will as a rule be later on the reaction path where the reaction path curvature is higher.[37] And, since higher barriers are often thinner,[38] an error in the calculated barrier may sometimes be correlated with an error in the calculated amount of tunneling. Nevertheless, we have found for the present case, as discussed below, that we draw similar conclusions about the interpretation of the kinetic isotope effect for all three semiempirical molecular orbital models, and this greatly increases our trust in the results.

Tunneling. Dewar et al.[15] calculated transmission coefficients from a very simple model and found 7.4×10^4 and 7.0×10^2 for the H- and the D-migration reaction, respectively, at 498 K. Chantranupong and Wildman[18] stated that, in their two-mode model, the H-migration rate constant would be 15 orders of magnitude smaller at 475 K in the absence of vibrationally assisted tunneling. The presently calculated SCT transmission coefficients are much smaller than these values; in particular they are in the range 3.7–4.9 for H migration and in the range 2.3–2.6 for D migration at 500 K. As just discussed, however, these calculations do account for the experimental observations.

We factorized the KIEs into the contribution from the tunneling factor κ^{SCT} and that from k^{CVT}, which corresponds to classical reaction-coordinate motion (see eq 2). In addition, we also calculated the ratios of the zero-curvature transmission coefficients for the H-migration reactions to those for the D-migration reactions. These factors and ratios are presented in Table IV. By comparing the KIEs calculated from k^{CVT} (which are 2.2–2.8) to those from $k^{CVT/SCT}$ (which are 3.8–5.7), one can see that the magnitude of the KIEs are very significantly affected by tunneling for all three parameterized models. Furthermore the KIEs calculated without tunneling increase only 6–7% over the temperature range in Tables III and IV, whereas those calculated with SCT tunneling increase 18–27% (compared to 13% for experiment). Thus tunneling can indeed account for the strong temperature dependence observed experimentally as well as for the magnitude of the KIEs.

Table IV. Factors in the Calculated KIEs

Hamiltonian	T (K)	$\frac{k_H^{CVT}}{k_D^{CVT}}$	$\frac{\kappa_H^{SCT}}{\kappa_D^{SCT}}$	$\frac{\kappa_H^{ZCT}}{\kappa_D^{ZCT}}$
MINDO/3	463.25	2.57	1.74	1.28
	470	2.54	1.71	1.27
	478.45	2.50	1.67	1.26
	500	2.42	1.59	1.23
AM1	463.25	2.28	2.27	1.68
	470	2.25	2.19	1.65
	478.45	2.22	2.10	1.61
	500	2.15	1.92	1.53
PM3	463.25	2.83	2.00	1.73
	470	2.81	1.94	1.70
	478.45	2.76	1.87	1.66
	500	2.65	1.73	1.57

Arrhenius Parameters. We calculated phenomenological Arrhenius parameters in all cases by fitting the calculated CVT and CVT/SCT rate constants at 463.25 and 500 K. Table V gives the Arrhenius parameters A_H and $E_{a,H}$ for the H-migration case and also A_H/A_D and $E_{a,D} - E_{a,H}$. When tunneling is included, the predicted difference in the activation energies is about three to four times the value calculated without considering tunneling effects. Furthermore, the ratio of the preexponential factors calculated with tunneling is a factor of 2–4 less than the value calculated without tunneling. Such comparisons show again that the strong temperature dependence of the KIEs is due to tunneling. Similar behavior of the difference in the activation energies and of the ratios of the preexponential factors are reported by Pegg and Meehan for the homodienyl sigmatropic [1,5] hydrogen shifts of [hydroxymethyl]styrylcyclopropanes.[22]

The suggestion of Jensen and Houk[14] that calculations without tunneling can account for the observed activation parameters, except for quantitative discrepancies caused by unconverged frequencies, is incorrect. Consider, e.g., the AM1 calculations for the H-migration case. If we calculate phenomenological Arrhenius parameters from our CVT/SCT rate constants at 463.25 K and 500 K and then repeat the calculation without tunneling (i.e., using CVT rate constants), we get an error of 5.9 eu in the entropy of activation and an error of 4.5 kcal/mol in the enthalpy of activation. Repeating the same test of the nontunneling model with the PM3 Hamiltonian yield errors of 5.2 eu for $\Delta S^{\ddagger}$ and 4.0 kcal/mol for $\Delta H^{\ddagger}$.

Discussion

Kinetic isotope effects have long been used by experimentalists to infer the properties of transition states by assuming that the dynamical bottlenecks of reactions involving different isotopes are the same, and therefore the classical potentials and force fields are the same. Typically tunneling effects are neglected as well. As mentioned previously, the variational effect is found to be negligible in the present calculations so the first assumption appears valid for the present reaction as far as overbarrier processes are concerned, but tunneling is not negligible.

(37) Eyring, H.; Lumry, R.; Spikes, J. D. In *A Symposium on the Mechanism of Enzyme Action*; Johns Hopkins Press: Baltimore, 1954; p 123. Hammond, G. S. *J. Am. Chem. Soc.* **1955**, *77*, 334. Mok, M. H.; Polanyi, J. C. *J. Chem. Phys.* **1969**, *51*, 1451.

(38) Marcus, R. A. *J. Phys. Chem.* **1968**, *72*, 891. More O'Ferrall, R. A.; Kouba, J. *J. Chem. Soc., B* **1967**, 985. Parr, C. A.; Truhlar, D. G. *J. Phys. Chem.* **1971**, *75*, 1844.

Table V. Arrhenius Parameters

	A_H (s^{-1})		$E_{a,H}$ (kcal/mol)		A_H/A_D		$E_{a,D} - E_{a,H}$ (kcal/mol)	
	CVT	CVT/SCT	CVT	CVT/SCT	CVT	CVT/SCT	CVT	CVT/SCT
MINDO/3	5.3×10^{10}	7.6×10^{9}	42.9	39.7	1.1	0.54	0.8	2.0
AM1	3.8×10^{10}	1.9×10^{9}	37.2	32.7	1.0	0.24	0.7	2.8
PM3	7.2×10^{11}	5.3×10^{10}	33.7	29.7	1.1	0.30	0.9	2.7

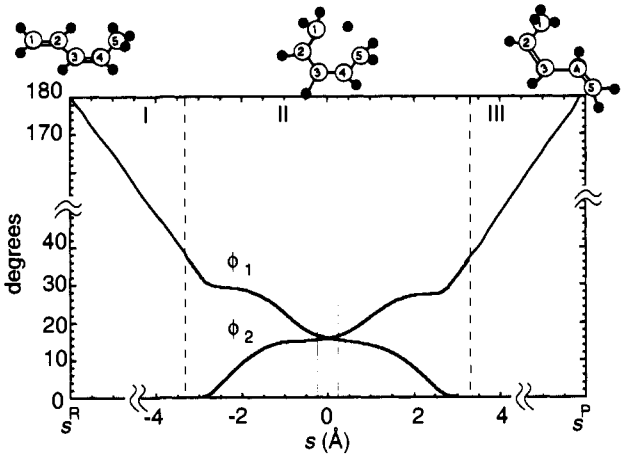

Figure 3. Dihedral angles as functions of the reaction coordinate. The thin vertical lines denote the same regions (the representative tunneling region) as indicated by thin vertical lines in Figure 4, for ease of comparison. The dashed vertical lines divide the reaction into three stages, I, II, and III. Schematic plots of the molecular structure at each stage are given along the top edge of the plot. ϕ_1 is the C1–C2–C3–C4 dihedral angle, and ϕ_2 is the C2–C3–C4–C5 dihedral angle. The plots of ϕ_1 and ϕ_2 are quantitative representations of the AM1 calculations in section II and are schematic in sections I and III.

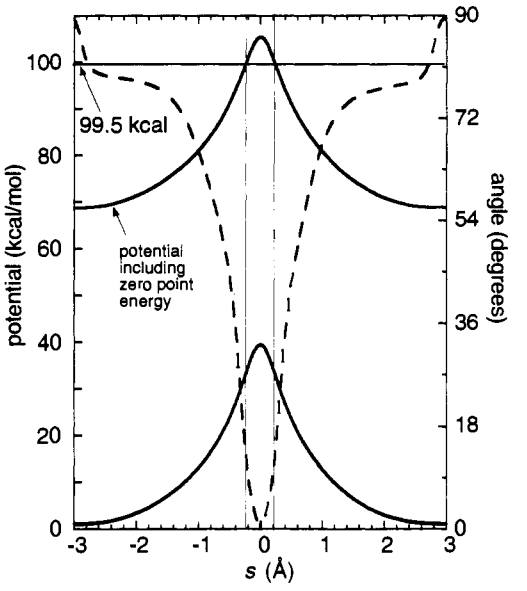

Figure 4. The top solid curve is the adiabatic ground-state potential energy profile $V_a^G(s)$ versus reaction coordinate obtained from AM1 for the H-migration reaction. The adiabatic ground-state potential energy curve is the sum of the potential energy along the minimum-energy path and the local zero-point energy. The horizontal line indicates the representative tunneling energy, at which the SCT tunneling probability is 1.1×10^{-2} (it is 0.5 at the top of the barrier). The vertical thin lines denote the reaction-coordinate turning points at this energy. The lower solid curve is the Born–Oppenheimer potential. The dashed curve is the angle between the mass-scaled minimum energy path and the imaginary-frequency normal mode of the saddle point; the scale for this curve is at the right.

Since results from all three Hamiltonians agree qualitatively, we next present a detailed analysis of the dynamical process of this reaction, in particular the nature of the tunneling process, for calculations with the AM1 Hamiltonian. Following that we compare the results from the three Hamiltonians.

The rearrangement reaction clearly involves rotation about the C2–C3 single bond. Following the minimum energy path down from the saddle point leads to an *s-cis*-type stationary point; thus—in the reverse process of climbing the hill—the reaction path passes through an *s-cis* conformation on the way from the *s-trans* one to the saddle point. Thus we can divide the reaction progress into three stages. These three stages are indicated by regions labeled I, II, and III in Figure 3. Regions I and III are schematic, and region II is from the AM1 calculation of the H-migration reaction. Since s measures a distance along a curved MEP whose character changes as a function of reaction progress, it bears no direct relation to any individual internal coordinate. Figure 3 shows the C1–C2–C3–C4 and C2–C3–C4–C5 dihedral angles, ϕ_1 and ϕ_2, respectively, versus the reaction coordinate s. Starting from the *s-trans* conformation, the ethylene group rotates about the C2–C3 single bond in region I; this involves a large-amplitude motion of ϕ_1. When the ethylene group is near the C5 methyl group, both ϕ_1 and ϕ_2 change in a concerted fashion. In the last stage, the C5 vinyl group rotates away from the C1 methyl group, and eventually the C3–C4 bond becomes *s-trans*.

Figure 4 shows three quantities versus the reaction coordinate within region II: the solid curves are the adiabatic ground-state potential energy profile and the classical potential energy barrier; the dashed curve is the angle between the MEP and its initial direction at the saddle point in the mass-scaled Cartesian coordinate system (which will be explained in detail below). At s = 3.0 Å, ϕ_1 is about 33°, which is very close to the 35° of the *s-cis* conformation. Thus the change of conformation to *s-cis* is essentially complete while the system is still in the foothills.

The energy which makes the largest contribution to the integral in eq 5 for the SCT transmission coefficient at 470 K is indicated by the horizontal thin line. This energy is called the representative tunneling energy[39] at a given temperature. It dominates the integral as a result of the competition between the decrease in the Boltzmann factor and the increase in the tunneling probability as the tunneling energy increases. There are two points, s_l and s_r, on the reaction path at which the adiabatic ground-state energy, $V_a^G(s_l)$ and $V_a^G(s_r)$, equals the representative tunneling energy (see eq 9). These are the termini of the representative tunneling path, and they can be viewed as defining the range of the MEP where tunneling is most likely to occur. This important range is indicated by two vertical thin lines passing through s_l and s_r in both Figures 3 and 4 as well as several later figures. It is clear from these figures that tunneling occurs in a very small vicinity of the saddle point, and that the two dihedral angles, ϕ_1 and ϕ_2, change about only 0.9° within this range.

Figure 5 gives the structures at s_l and s_r for the representative tunneling energy and shows that they are very close to the symmetric structure which is the saddle point. More precisely, the only significant difference (~0.2 Å) in the structure is the distance between the hydrogen atom that is transferred and the two carbon atoms, C1 and C5. Thus the tunneling mode is a C1–H–C5 asymmetric stretch. This is consistent with the character of the imaginary normal mode eigenvector at the saddle point.

Figure 6 presents the vibrational frequencies of the generalized normal modes versus the reaction coordinate (note that the imaginary normal mode at the saddle point is not included because it is the reaction coordinate). Because of the multitude of avoided crossings, these generalized normal modes exhibit strong couplings at various points along the reaction path. However, if we make

(39) Kim, Y.; Truhlar, D. G.; Kreevoy, M. M. *J. Am. Chem. Soc.* **1991**, *113*, 7837.

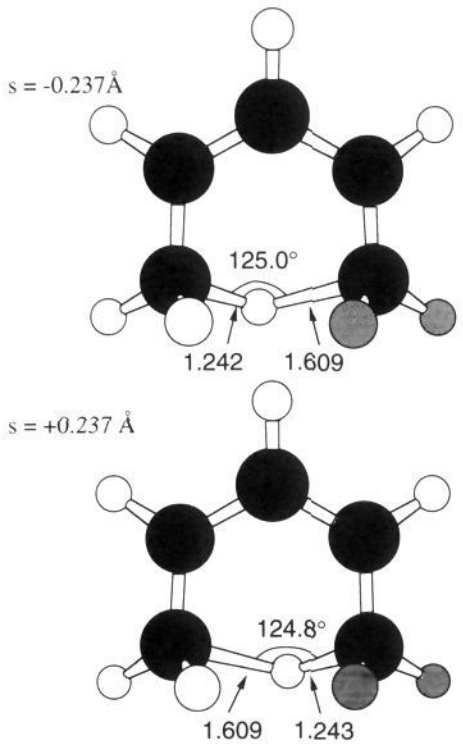

Figure 5. Structures of the system at the representative tunneling path termini in the AM1 calculation for the H-transfer reaction. The dark circles denote carbon atoms, the gray circles denote deuterium, and the open circles represent hydrogen. Distances along the reaction path and the values of the making and breaking bond lengths are indicated in Å.

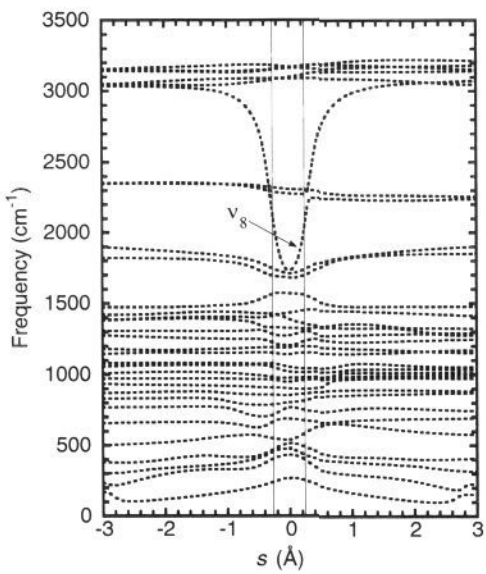

Figure 6. The generalized normal mode frequencies versus the reaction coordinate. The thin vertical lines delimit the same representative tunneling region as in Figures 3 and 4.

a diabatic correlation,[40] we see that one of the calculated C–H stretch modes decreases from 3038 cm^{-1} to 1730 cm^{-1} at the saddle point, where it becomes primarily at C2–C3–C4 skeletal asymmetric mode.

It is clear from the figures that the reaction path has turned into the asymmetric stretch of the C–H–C motion at s_l and s_r. Our calculations indicate that a noncollinear tunneling path preceded by a classical internal rotation explains the KIEs. We may conclude that the low-frequency internal rotational mode

(40) Truhlar, D. G.; Isaason, A. D. *J. Chem. Phys.* **1982**, *77*, 3516.

Table VI. Percentage Contribution to Reaction Path Curvature

mode[a]	s = −0.26 Å	s = −0.10 Å	s = 0.10 Å	s = 0.26 Å
ν_1–ν_7	0	1	1	6
ν_8	66	31	27	62
ν_9–ν_{27}	30	52	54	26
ν_{28}–ν_{32}	4	16	18	6

[a] When a range is shown, the percentage refers to the sum of the percentage contributions over that set of modes.

assists the early stage of classical motion along the reaction path, but it is not involved in the process of tunneling. There is, however, some coupling of skeletal modes to the reaction coordinate, which accounts for κ^{SCT} being larger than κ^{ZCT}.

It is interesting to compare the dynamical picture that emerges from the present calculations to the model used by Chantranupong and Wildman[18] who also used the AM1 Hamiltonian. They used a two-dimensional model which includes an antisymmetric methyl stretching mode and a skeletal mode. The frequency for the antisymmetric stretching mode was taken from experiment, and the reduced mass was assigned to 1 and 2 amu for the H- and the D-migration reactions, respectively. The reduced mass for the skeletal mode was fixed to the value for the lowest frequency A′ mode in the C_s symmetry, and the frequency of this mode was varied to fit the experimental KIE at 475 K. The assumption in this two-mode approach is that the lowest frequency A′ mode is one of the degrees of freedom that participates most strongly in the tunneling process.

In order to test their assumptions, we examined the modes that contribute the most to the reaction-path curvature, since the implicit tunneling path[1a] of the centrifugal-dominant small-curvature approximation[9] may be approximated[26c] by a curve connecting the classical vibrational turning points along the curvature direction on the concave side of the MEP. We first label the 32 bound modes orthogonal to the reaction path as ν_1, ..., ν_{32} in order of decreasing frequency. The frequencies of these modes are shown in Figure 6. The mode singled out in the two-mode model of Chantranupong and Wildman is ν_{31} in this notation, i.e., the second-lowest frequency; this mode involves primarily motions of the hydrogens on C1 and C5. Table VI shows the percentage contributions of various subsets of the 32 modes to the reaction-path curvature at four points within the region of the MEP corresponding to the representative path, i.e., in the region between −0.237 to 0.237 Å. To make this table, the projection of the curvature vector onto each normal mode was divided by the norm of the curvature vector and converted to a percentage. Table VI shows that mode 31 and the four other modes below 600 cm^{-1} couple very little to the reaction path in the representative tunneling region. The mode coupling most strongly to the reaction path in this region is mode ν_8, which is primarily a hydrogenic motion on C5 at s = −0.1 Å and on C1 at s = +0.1 Å, but is a C2–C3–C4 asymmetric stretch near s = 0. The reaction path is an asymmetric C1–H–C5 stretch throughout this region.

We tested whether the reaction may be treated as a small-curvature case by also calculating the transmission coefficients by a large-curvature[9,10,41] tunneling approximation. This yielded smaller transmission coefficients, which is an indication that the small-curvature approximation is valid. To further assess the probable validity of the SCT approximation for this reaction, consider the angle between the imaginary-frequency normal mode eigenvector at the saddle point and the gradient at each s, as shown in Figures 4 and 7. Figure 7 is a blowup of the region near the barrier top of Figure 4. Figure 7 shows that the angle between the MEP and the imaginary frequency normal mode eigenvector at the saddle point (which determines the initial direction of the MEP as the system leaves the saddle point) changes very little over the region covered by the representative tunneling process. This angle represents approximately the amount that the MEP has curved away from a straight line due to the reaction-path

(41) Truhlar, D. G.; Lu, D.-h.; Tucker, S. C.; Zhao, X. G.; Gonzalez-Lafont, A.; Truong, T. N.; Maurice, D.; Liu, Y.-P.; Lynch, G. C. *ACS Symp. Ser.* **1992**, *No. 502*, 16.

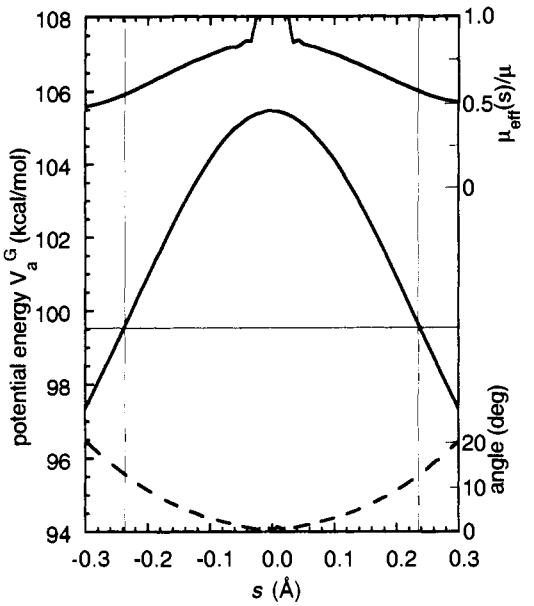

Figure 7. Same as Figure 4, but for a smaller region around the barrier top. Also, the scale for the angle between the MEP and the imaginary frequency eigenvector is moved to the lower right, and another reaction-path function, $\mu_{eff}(s)/\mu$, is shown with a scale in the upper right. The thin vertical lines delimit the same representative tunneling region as in Figures 3, 4, and 6.

curvature. At s_1 and s_r, this angle is about 13°. Therefore, the reaction path curves about 27° in proceeding from the beginning to the end of the representative tunneling path. This confirms that the reaction is a small-curvature case. Figure 7 also shows the ratio of the effective reduced mass to the reduced mass.

Certain details of the dynamics are not the same for the three parameterized models. We have already discussed that barrier heights obtained from the three Hamiltonians are very different and that the absolute reaction rate constants from the three Hamiltonians differ by several orders of magnitude. When reaction-path curvature is neglected, the PM3 method shows the most tunneling; this can be explained by the fact that this Hamiltonian gives the thinnest barrier, as shown in Figure 8. The coupling between the reaction path and the generalized normal modes due to the reaction-path curvature is also quite different in the three cases. This effect can be observed in the enhancement of the tunneling contribution to the KIEs when increasing the level of theory from the ZCT to the SCT approximation. Such coupling is stronger in the case of MINDO/3 (29–36%) and AM1 (25–35%) than for PM3 (10–16%). This occurs because the MEP curves through an angle of only about 6° in the representative tunneling process of the PM3 calculation, as compared to 16° in the AM1 calculation and 18° in the MINDO/3 case. The effective reduced masses are 0.74 amu, 0.93 amu, and 0.56 amu for AM1, PM3, and MINDO/3, respectively, at the reaction-coordinate turning point for the representative tunneling energy at 470 K. Because of the strong coupling and because of the thinner barrier, AM1 gives the largest tunneling contribution to the KIEs when reaction-path curvature is included. The quantitative validity of our treatment of this reaction is limited to those characteristics for which the errors in the PEFs are canceled for different isotopes. The differences between the results obtained from the three Hamiltonians illustrate a long-standing problem—the dependence of *detailed* dynamics on accurate modeling of the force field.

It is encouraging that a general dynamics method without any ad hoc assumptions can achieve good agreement with experiment.

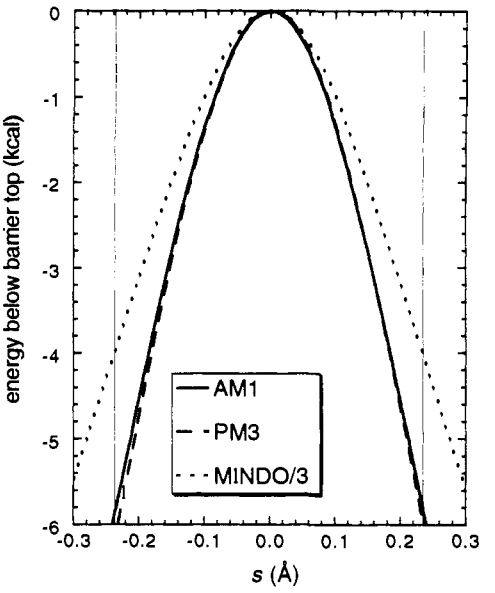

Figure 8. The adiabatic potential $V_a^G(s)$ with respect to V_a^{AG} at each s for the three Hamiltonians. The thin vertical lines delimit the same representative tunneling region as in Figures 3, 4, 6, and 7. Note that V_a^{AG} is defined as the maximum of the $V_a^G(s)$ curve.

The semiqualitative agreement between all three Hamiltonians is also encouraging. We are especially encouraged by the success of this full-dimensional calculation because conclusions drawn from calculations may be more objective when a full dimensionality method is applied. A valuable aspect of the semiclassical model used here is that it shows which regions of the potential energy surface are most critical for the results, e.g., the geometries at the start and end of the representative tunneling path, and this provides qualitative guidance about where to begin in refining the model. Our results show that certain dynamical properties are very sensitive to the global features of the force field, and we need more reliable calculations of such surface features to better understand the dynamics. Furthermore, this kind of feature should be included in the parameterization to achieve useful accuracy in dynamics predictions.

Conclusion

We have shown that the experimental kinetic isotope effects (KIEs) for the [1,5] sigmatropic rearrangement of *cis*-1,3-pentadiene can be understood by a general treatment, namely, variational transition-state theory with a multidimensional tunneling approximation. We also demonstrated the applicability of *direct dynamics* to large chemical systems (13 atoms). The semiqualitative agreement between a full 13-atom calculation and experiment, without adjusting parameters to kinetic data, is very encouraging for our future ability to model KIEs in complex systems. Although there are some unresolved quantitative differences between results from different semiempirical molecular models, the qualitative and semiquantitative agreement of the various semiempirical molecular orbital parametrizations has provided us confidence in the conclusions drawn from the analysis.

Acknowledgment. The authors are grateful to Chris Cramer, Rick Randall, and Robert Topper for helpful discussions. This work was supported in part by the Division of Chemical Sciences, Office of Basic Energy Sciences, U.S. Department of Energy by Grant DE-FG02-86ER13579 from the Office of Energy Research to D.G.T. at the University of Minnesota and by Contract No. DE-AC06-76RLO 1830 with Battelle Memorial Institute which operates the Pacific Northwest Laboratory.